Water Resources Research

RESEARCH ARTICLE
10.1029/2023WR036164

Examining the Mid to Long-Term Variability in Saturated Hydraulic Conductivity of Sandy Soils and Its Influencing Factors Under Constant Head Test in the Laboratory

Saeed Nikghalb Ashouri[1], Adrian Pittari[2], Vicki Moon[2], and Ali Shokri[1]

[1]School of Engineering, University of Waikato, Hamilton, New Zealand, [2]School of Science, University of Waikato, Hamilton, New Zealand

Key Points:

- The estimation of saturated hydraulic conductivity through constant head tests demonstrates sensitivity to the duration of the tests
- Observations indicate an alteration in particle size distribution before and after testing within different sections of the samples
- Flow rate and hydraulic gradient vary over the test duration, emphasizing the complex hydraulic system within the samples

Correspondence to:

A. Shokri,
ali.shokri@waikato.ac.nz

Citation:

Nikghalb Ashouri, S., Pittari, A., Moon, V., & Shokri, A. (2024). Examining the mid to long-term variability in saturated hydraulic conductivity of sandy soils and its influencing factors under constant head test in the laboratory. *Water Resources Research*, *60*, e2023WR036164. https://doi.org/10.1029/2023WR036164

Received 6 SEP 2023
Accepted 21 SEP 2024

Author Contributions:

Conceptualization: Saeed Nikghalb Ashouri, Ali Shokri
Data curation: Saeed Nikghalb Ashouri, Ali Shokri
Formal analysis: Saeed Nikghalb Ashouri, Ali Shokri
Investigation: Saeed Nikghalb Ashouri, Ali Shokri
Methodology: Saeed Nikghalb Ashouri, Ali Shokri
Supervision: Ali Shokri
Validation: Saeed Nikghalb Ashouri, Ali Shokri
Visualization: Saeed Nikghalb Ashouri, Ali Shokri
Writing – original draft: Saeed Nikghalb Ashouri
Writing – review & editing: Adrian Pittari, Vicki Moon, Ali Shokri

Abstract Saturated hydraulic conductivity (*Ks*) is a crucial parameter that influences water flow in saturated soils, with applications in various fields such as surface water runoff, soil erosion, drainage, and solute transport. However, accurate determination of *Ks* is challenging due to temporal and spatial uncertainties. This study addresses the knowledge gap regarding the long-term behavior of *Ks* in sandy soils with less than 10% fine particles. The research investigates the changes in *Ks* over a long period of constant head tests and examines the factors influencing its variation. Two sandy samples were tested using a hydraulic conductivity cell, and the hydraulic head and discharge were recorded for over 50 days. The results show a general decline in *Ks* throughout the test, except for brief periods of increase. At the end of both tests, there are noticeable reductions in the saturated hydraulic conductivities of the samples, with one sample being 96% and the other sample 91% less than the maximum recorded saturated hydraulic conductivity during the tests. Furthermore, the relationship between flow rate and hydraulic head gradient does not follow the expected linear correlation from Darcy's law, highlighting the complex nature of sandy soil saturated hydraulic conductivity. The investigation of soil properties in three different sections of the samples before and after the tests revealed a decrease in the percentage of fine particles and a shift in specific gravity from the bottom to the top of the sample, suggesting particle migration along the flow direction. Factors such as clogging by fine particles and pore pressure variation contribute to the changes in *Ks*. The findings of this research show the importance of considering changes of saturated hydraulic conductivity during constant-head laboratory tests. Therefore, this study provides evidence for the requirement to further assess the laboratory methods for measurement of the saturated hydraulic conductivity in sandy soil mixtures.

1. Introduction

The saturated hydraulic conductivity (*Ks*) plays a crucial role in determining the water flow rate within the saturated zone of soils. This parameter is essential in various fields of study, including surface water runoff, soil erosion, deep percolation, drainage, crop simulation models, and solute transport (Ben-Hur et al., 2009; Boadu, 2000; Hwang et al., 2017; Suleiman & Ritchie, 2001). Using the Darcy equation, *Ks* can be defined as the ratio of water flow (*Q*) in the unit section of saturated soil (*A*) to the hydraulic gradient (*i*). The parameter *Ks* is present in the majority of equations related to water flow in a saturated medium, yet its determination can be challenging both in the laboratory and the field due to temporal and spatial uncertainties (Suleiman & Ritchie, 2001).

Laboratory determination of *Ks* utilize three standard methods: constant head, falling head, and constant flow rate, as detailed in ASTM D5856-15 (2015). When dealing with granular and disturbed samples containing less than 10% of fine particles passing 75 μm or No. 200 sieve, the recommended approach is the constant head method, as outlined in ASTM D2434-19 (2019). Conversely, samples comprising more than 10% of fine particles can be analyzed using any of the three mentioned methods. However, *Ks* measurements are conducted using a rigid-wall, compaction-mold permeameter, with specific criteria provided in ASTM D5856-15 (2015).

Extensive research has been conducted on the long-term variations of saturated hydraulic conductivity in low-permeability soils, which are commonly employed in landfill sites and artificial wetlands. From the perspective of an Earth scientist, these materials might be perceived as loose sediment or deposits rather than the conventional 'soil,' which typically encompasses a mixture of inorganic and organic constituents. In landfills, leachate, and artificial wetlands, contaminated water from roads needs to be contained to gradually remove the

pollutants from the water and prevent pollution of underground water resources (Fang et al., 2022; Li et al., 2023; Shaver, 2020; Touze-Foltz et al., 2006; Valencia-González et al., 2022; Wang et al., 2023). Therefore, the application of a layer with very low permeability is necessary to reduce the infiltration of contaminated water into the soil while simultaneously eliminating pollutants. Several studies have shown that the *Ks* in low permeability soil samples change with infiltration of the water that contains chemical or biological agents (Francisca & Glatstein, 2010; Liu & Liu, 2020; Lu et al., 2020; Montoro & Francisca, 2010).

Chemical substances present in the fluid can create a chemical imbalance and interfere with ion exchange processes in the soil, leading to fluctuations in *Ks*. According to a study conducted by Jo et al. (2005), a 3 year test observed a tenfold variation in *Ks* of a clay liner permeated by leachate-containing chemical agents. In their tests, the saturated hydraulic conductivity of one of the samples reached stability after about 1.5 years of the test. On the other hand, the formation of microorganisms and the presence of nutrients to feed them can cause clogging in the soil and, hence, a reduction in the drainable pores and *Ks* (Fang et al., 2022; VanGulck & Rowe, 2004).

In sandy soils, the duration of the test is usually relatively short. It is commonly assumed that the test can be concluded when four samples yield values within ±25% of the mean calculated from these four samples throughout the test (ASTM D5856-15, 2015). Also, there is no reference to the length of the test in ASTM D2434-19 (2019). However, several studies suggest that the saturated hydraulic conductivity of sandy soils can change over time. For example, there has been extensive research on the variation of saturated hydraulic conductivity in groundwater artificial recharge (Konikow et al., 2001; Mays & Hunt, 2005; Siriwardene et al., 2007; Song et al., 2020; Ye et al., 2019). Vanderzalm et al. (2020) and Du et al. (2018) subjected sandy samples to water permeation containing suspended solids and *Fe (III)* ions, respectively, for an extended period (40 days in the former case and 7 days in the latter study), leading to observed fluctuations in *Ks* that demonstrate a prevalent declining pattern over time. These studies identified physical and biological clogging mechanisms as dominant factors for *Ks* variation. However, neither of the above studies has tested a sample permeated with distilled water or tap water with minimum suspended solids or chemicals to ensure that *Ks* remains constant under minimum influent contamination. Du et al. (2013) and Wang et al. (2012) used tap water with and without suspended solids in a constant head test on quartz sand samples and observed a noticeable drop in *Ks* over 4 days. Siriwardene et al. (2007) also reported a reduction in the *Ks* when the sample was permeated with tap water containing suspended solids. They noticed clogging of the suspended solids in the lower section of the sample as the main reason for the noticeable drop in the *Ks*, whereas Wang et al. (2012) showed that finer suspended solids could travel deeper in the sample and cause blockage of the drainable pores.

Clogging can also be caused by the internal mobilization or swelling of fine particles in the soil (Jeong et al., 2018; Konikow et al., 2001; Mohan et al., 1993; Torkzaban et al., 2015). Additionally, clay minerals like *Illite*, *Kaolinite*, and *Montmorillonite* can be transported with water, leading to the blockage of drainable pores in the sample and a reduction in *Ks* (Cihan et al., 2022; Jeong et al., 2018; Wang et al., 2021). The migration of fine particles in soil is a phenomenon that occurs due to various factors such as seepage forces, hydraulic gradients, and soil deformation. Fine particle migration can lead to geotechnical damage, failures of earth dams and soil slopes, and changes in the properties of the soil. It has been observed that seepage forces induce the migration of fine soil particles along the water flow direction, causing redistribution and reconsolidation of sand particles (Wang et al., 2022). Dikinya et al. (2006) observed a substantial decrease in hydraulic conductivity due to structural breakdown and pore clogging caused by dispersion and re-deposition of fine particles.

In a research on the transportation of fine particles in petroleum and groundwater reservoirs, Tangparitkul et al. (2020) performed an analytical study on the mobilization of the fine particles and concluded that size distribution of the fine particles and velocity of the permeant fluid dominate the mobilization of the particles. Wang et al. (2022) studied the impact of the hydraulic gradient on seepage failure in sandy samples in a set of 15 min constant head tests and resulted that the distribution of particles in the samples change due to water flow, leading to transportation of fine particles to the top, and coarse particles to the bottom.

Stormwater management devices like artificial soakage basins and soak pits are commonly recommended in new urban developments with high infiltration rates (Shaver, 2020). Furthermore, with the widespread use of artificial groundwater recharge, the long-term behavior of *Ks* in sandy materials gains significant importance. Variations in *Ks* and pore blockages can profoundly influence the effectiveness of design strategies employed in stormwater management and groundwater recharge scenarios.

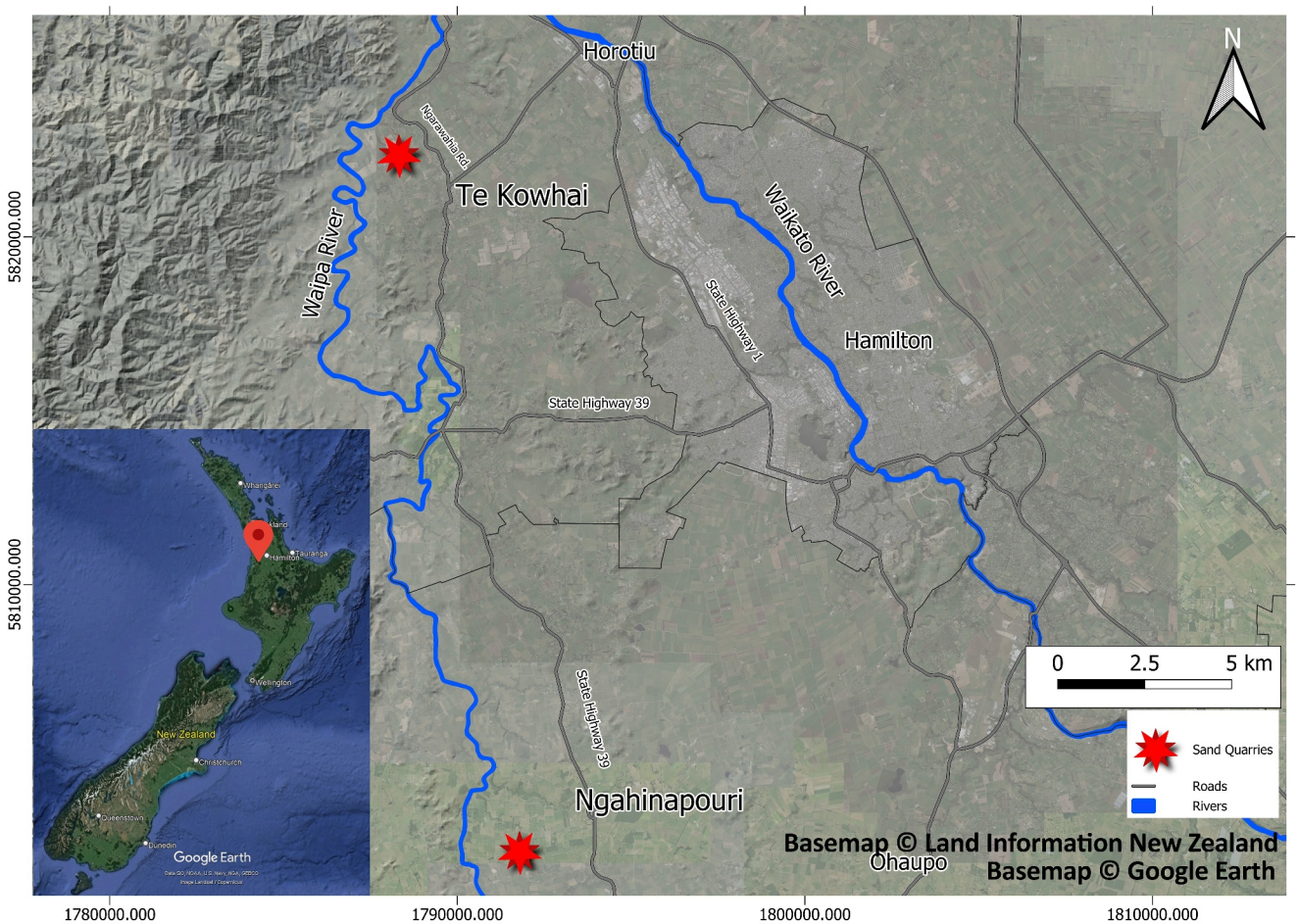

Figure 1. The geographical location of the Waipa River in New Zealand, with the samples originating from sand quarries located near the Waipa riverbanks. The locations of the sand quarries are approximate.

Currently, there is a lack of research focusing on the extended-duration variations in *Ks* within sandy soils due to fluctuating hydraulic levels. Observing *Ks* over the long term provides insights into the sustained groundwater movement within the aquifer, with changes in hydraulic levels indicating shifts in aquifer water levels during and after rainfall events. This study aims to bridge the knowledge gap regarding the prolonged behavior of saturated hydraulic conductivity in sandy soils. Although various research has explored short-term *Ks* variations, particularly in the context of stormwater management devices, a comprehensive understanding of how *Ks* evolves over extended timeframes remains limited. Grasping the mid to long-term behavior of *Ks* holds critical significance in modeling water flow and solute transport in the soil. Increasing the accuracy of estimates of the *Ks* provides better design of soakage systems and safeguarding subsurface water resources. Thus, this paper illuminates the key factors shaping *Ks* variations over prolonged periods.

2. Materials

2.1. Sample Source and Physical Properties

The soil examined in this study is river sand, commercially referred to as pit sand, often employed for embankments and raised areas like pathways. A batch of pit sand was purchased from a supplier in Hamilton, New Zealand, that provides different types of aggregates for garden and home purposes. According to the statement of the supplier, they acquire the pit sands from sand quarries situated in Ngahinapouri and Te Kowhai, located along the Waipa River in Waikato, New Zealand, as depicted in Figure 1. A bag of 10 kg of pit sand was purchased and brought to the laboratory, and the samples were prepared according to the procedure explained in the following

Table 1
Properties of Tested Samples

Parameter	Sample A	Sample B
Specific gravity of grains (−)	2.6739	-
Specific surface (m^2/kg)	84.60	102.90
Particles <5 μm (%)	2.3	2.6
Particles 5–75 μm (%)	5.06	5.83
Particles >75 μm (%)	92.61	91.56
Dry bulk density (g/cm^3)	1.289	1.261
Optimal gravimetric compaction moisture (%)	12	12
Sample gravimetric moisture (%)[a]	8.1	11.8
Organic matter (%)	1.7	1.7

[a]Sample gravimetric moisture was measured when the sample was compacted in the mold. A small amount of sample A and B was taken and dried in the oven, and moisture was measured.

section. For this study, two samples (sample *A* and sample *B*) were taken from the same batch of pit sand provided by a supplier.

Table 1 outlines the physical properties of the samples. Upon microscopic examination and particle separation, five distinct groups are discerned (Figure 2): quartz and feldspar (approximately 60%), pumice (approximately 11%), rock fragments and ferromagnesian minerals (approximately 6%), magnetic minerals (approximately 10%), and glass shards (approximately 13%). The magnetic minerals were isolated through magnetic separation. X-ray diffraction (XRD) analysis was employed to assess mineral composition, while the loss on ignition (LOI) method was utilized to estimate the presence of organic material in the samples. The analysis of XRD data peak patterns confirms that quartz and feldspar constitute the majority of minerals in the sample (Figure 3). The observed low dry bulk density can be attributed to the presence of pumice within the samples (Table 1). As per the Digital Soil Map (SMAP) database, the dry bulk density of deposits along the banks of the Waipa River typically spans from 0.8 to 1.3 g/cm³ (Landcare Research, 2023). The dry bulk density values of the analyzed samples align within the aforementioned range. Given that the samples are derived from the same batch, it is assumed that both samples A and B exhibit comparable specific gravity (Gs). The Gs (which is density of grains proportional to the density of water) was determined as the average value derived from five measurements conducted using a gas pycnometer.

A laser diffractometer (Malvern Mastersizer 3,000, Malvern Instruments Ltd., UK) was used to determine the particle size distribution of the samples. For this study, the particles below 75 μm were considered as fines, which aligns with the classification of ASTM for fine and coarse particles (ASTM D2487, 2020). The particle size distribution results indicate that the samples are primarily sandy, with less than 10% of fine materials. Particles below 5 μm were considered mobile colloidal particles (Kretzschmar et al., 1999), and the percentages of these particles are also mentioned in Table 1. Based on Standard Proctor tests (ASTM, 2012), the optimal compaction moisture of the samples was determined to be 12% by mass.

3. Methods

3.1. Sample Preparation

Prior to conducting the tests, the samples underwent a preparation process that involved drying in an oven at 105°C for 24 hr and passing through a 2 mm sieve. The moist tamping method was used to prepare the samples, which is based on a technique described by Ladd (1978). This method allows for achieving a uniform distribution of density in the sample. A specific amount of soil was weighed, and distilled water was sprayed onto the samples to attain an initial moisture content of 8.1% (Sample A) and 11.8% (Sample B). The choice of 8.1% moisture for sample A was intended to explore the influence of initial compaction moisture on the extended-term variations of

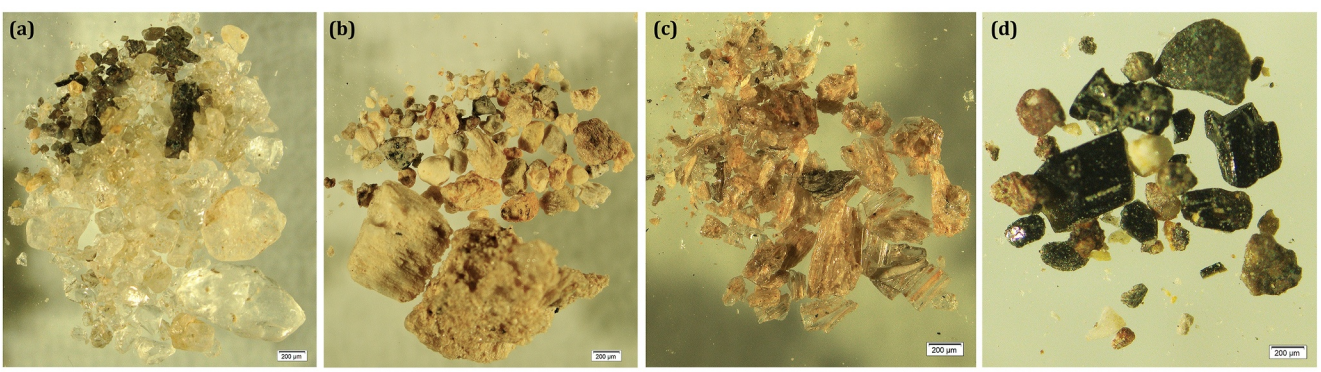

Figure 2. Separation of particles under microscope: (a) Quartz and feldspar, (b) Pumice, (c), glass shards, and (d) rock fragments and ferromagnesian minerals, and magnetic minerals - The magnetic minerals were separated by magnet, but there is not a separate picture of them.

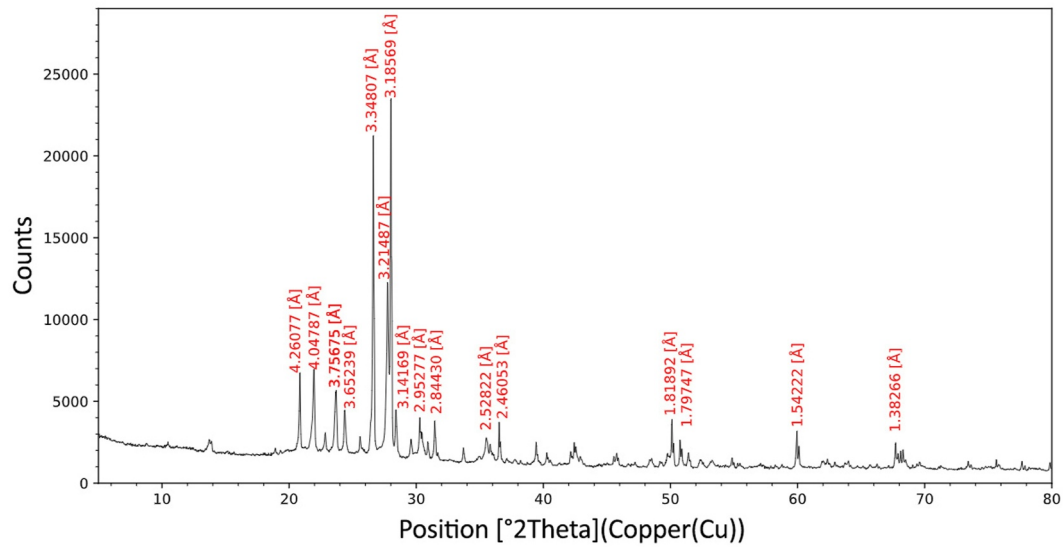

Figure 3. XRD analysis of the sample: Major peaks are related to the quartz and feldspar content in the sample.

Ks. The samples were then covered and left for approximately 24 hr to achieve moisture balance before testing. The samples were compacted in a constant head test cell with an interior diameter and height of 76.2 and 292 mm, respectively. Compaction was carried out in layers of 12 mm. Before the compaction, subsamples were taken to measure the actual moisture, particle size distribution, and XRD. The final dry density of the samples was calculated from the net dry soil used and compacted sample volume, and is listed in Table 1.

To achieve saturation, the samples were first connected to a vacuum pump for 1 hour. Distilled and de-aired water was then introduced into the test cell in an upward direction, following the procedure outlined in ASTM D2434-19 (2019), to minimize air entrapment. The samples were left saturated overnight to reduce the chances of air entrapment further.

3.2. Constant Head Saturated Hydraulic Conductivity Tests

The schematic experimental apparatus used for the constant head saturated hydraulic conductivity test is shown in Figure 4. The adjustable water head tank enabled the alteration of the hydraulic head during the experiment without the need to terminate the test. In addition, there were porous disks with a 1 mm mesh size and a spring on top to hold the sample stable in the cell. The mesh size of the porous disk was selected in a way to prevent the formation of clogging and pressure drops on the disk.

The water flow and head gradient were measured at least thrice daily. The collection of effluent in a bucket was carried out for each flow measurement, and the duration of the effluent collection was recorded. Subsequently, the discharge was calculated by dividing the weight of the collected effluent by the collection duration.

Formation of air bubbles during the test can change *Ks*. However, because the *Ks* of the sandy soils is relatively high compared to the silty and clayey soils, it was not possible to provide de-aired water for the whole period of the tests. In order to minimize the air entrapment during the test, permeation was from bottom to the top so that the air bubbles can escape. The samples were also regularly checked during the test for formation of any air bubbles in the transparent cell.

The tests were conducted in a back-and-forth pattern with water heads ranging from 963 to 1,765 mm, with increments and decrements of approximately 200 mm. The hydraulic head began at a minimum of 963 mm and was incrementally increased by around 200 mm until it reached a maximum of 1,765 mm. Subsequently, the head followed the same pattern of decrease in sequential steps. The testing period has lasted for approximately 53 days. Detailed information on the test phases, hydraulic heads, and durations can be found in Table 2. The tests were conducted in a laboratory with controlled temperature. Throughout the tests, the temperature variations were below 4°C. Consequently, the potential impact of temperature changes on *Ks* can be deemed negligible.

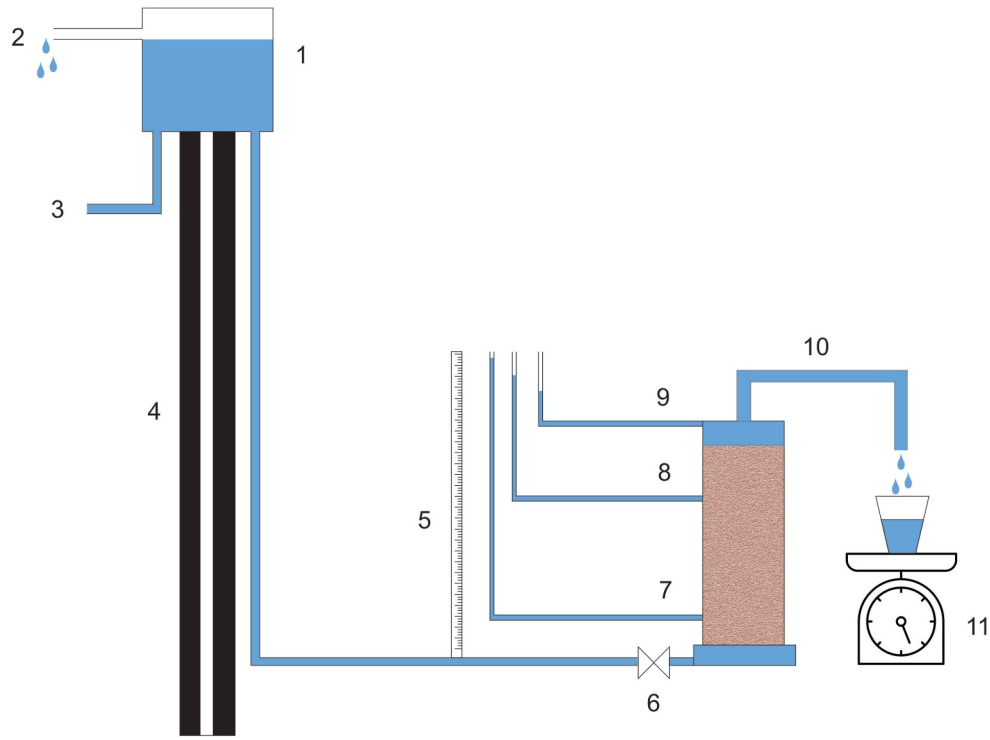

Figure 4. Schematic constant head saturated hydraulic conductivity apparatus-(1) Water tank, (2) overflow outlet, (3) water supply hose, (4) adjustable level board, (5) ruler, (6) water entrance valve, (7) piezometer 1, (8) piezometer 2, (9) piezometer 3 (10) water outlet (11) scale for measuring the discharge.

The hydraulic heads applied in this research are not representative of the place where the samples are originated. Since the pit sand is used in disturbed form for construction work as filter material to facilitate infiltration of water, it will be under different head gradients depending on the storm events and subsurface water levels. Therefore, the hydraulic gradients were selected to cover a wide range.

During the testing process, the pressure and discharge readings were recorded simultaneously by three piezometers. As depicted in Figure 4, the pressure inside the sample was measured by two piezometers located at points seven and eight, while the piezometer at point nine measured the water head at the discharge point on the opposite end of the cell.

In order to minimize the systematic error which results from measurement devices, including measurement of discharge by weight, and reading of the water heads in the piezometers, each reading set of discharge and head was done twice, and the mean value was used for calculating the *Ks*. If the difference between two reads was more than 1%, then the discharge and heads were measured for the third time. And the final *Ks* in each read would be the mean of the two closest measurements.

To minimize the accidental changes in the *Ks*, the constant head hydraulic conductivity system was set up in a laboratory with limited access, with warning signs so that unauthorised individuals do not touch the cell accidently.

Table 2
Hydraulic Head and Durations of Constant Head Tests on Samples A and B

Test phase	1	2	3	4	5	6	7	8	9	10
Hydraulic head (mm)	963	1,163	1,365	1,558	1,765	1,558	1,365	1,163	963	Varies
Sample A Duration (days)	5	6	6	6	5	3	7	6	7	1
Sample B Duration (days)	5	5	5	5	5	5	5	5	31	N/A

After completing Phase 9 on sample *A*, the water flow was not stopped, and a moderately rapid constant head test was conducted using the same hydraulic heads as phases 1 to 9. This phase, designated as "Phase 10", and as mentioned, continued from end of Phase 9, lasted approximately 16 hr, with each constant head being run for about 2 hr. The purpose of Phase 10 was to observe any changes in *Ks* under a shorter duration and to determine if the *Ks* during the head-increasing stage were similar to the reciprocal *Ks* during the head-decreasing stage.

In the case of sample *B*, Phase 9 was allowed to run for 31 days at the minimum head (963 mm) after an increasing trend in the *Ks* of the sample was observed from day 53 onwards. The purpose was to determine how long the *Ks* would continue to change and whether it would return to a value similar to the beginning of the test.

The *Ks* was calculated using Darcy's law (Wang et al., 2020) as follows (Equation 1):

$$K_s = \frac{Q}{i.A} \tag{1}$$

where *Ks* is the saturated hydraulic conductivity of the sample (m/s), *Q* is the rate of flow in the sample (m^3/s), *i* is the hydraulic gradient (m/m), and *A* is the cross-sectional area of the sample (m^2).

3.3. Post-Processing of the Samples

In order to examine changes in soil properties before and after the tests, the samples were recovered from the saturated hydraulic conductivity cell. After extraction, the samples were divided into three sections: bottom, middle, and top. Sub-samples were extracted from these sections to perform further analysis. In order to ensure the sub-samples are representative of the sections that they belong to, minimum of five sub-samples at each section were utilized for particle size distribution (PSD) and specific gravity (Gs) measurements.

The sub-samples were dried in the oven for 24 hr. Measurements of Gs were carried out by a gas pycnometer (Ultra Pycnometer 1,000- Anton Paar QuantaTec Inc., USA). Five samples from each section were separated to measure the Gs and each measurement was repeated four times in the pycnometer. Therefore, 20 measurements for each section were recorded. In order to measure the particle size distribution, a laser diffractometer was used (Malvern Mastersizer 3,000, Malvern Instruments Ltd., UK) and five measurements were recorded for each section.

Fine particles can mobilize with water flow and leave the system. In order to measure the fine particles leaving the system, two approaches were considered: Particle size analysis before and after the tests; measurement of the weight of the saturated cells before and after the tests. There could be another approach that includes installing a very fine mesh in the outlet pipe. However, there was the risk of blockage in the outlet pipe, and as a result, the whole test could have failed. Therefore, the latter approach was not applied.

4. Results

4.1. Mid to Long-Term *Ks* Test

The mid to long-term change in *Ks* calculated for both samples is illustrated in Figure 5. The *Ks* values of the samples showed a general decline throughout the test, as shown in Figure 5, except for three brief periods. These periods occurred between days 36–38 for sample *A* and between days 0–1 and 37 to 40 for sample *B*.

Furthermore, there are two distinct periods of a noticeable increase in *Ks* in both samples, which coincide closely in timing, specifically between days 35 and 40. In sample *A*, the increase in *Ks* starts at 1,365 mm head and ends at the same head in Figure 5a. However, in sample *B*, *Ks* starts increasing at 1,163 mm head and starts decreasing again at 963 mm head in Figure 5b. At the end of the tests on sample A, the final Ks value reaches to 0.5×10^{-4} m/s approximately that is 96% less than the maximum value (12.3×10^{-4} m/s). In sample B, the final Ks is 1×10^{-4} m/s approximately that is 91% less than the maximum value (12.2×10^{-4} m/s). Figure 5 illustrates that sample *A*, with initial moisture of 8.1%, achieved its maximum *Ks* within the first few hours of commencing the test. In contrast, sample *B,* with the initial moisture of 11.8%, took approximately 2 days to reach its peak *Ks*. From the peak point onwards, the *Ks* followed a reducing trend.

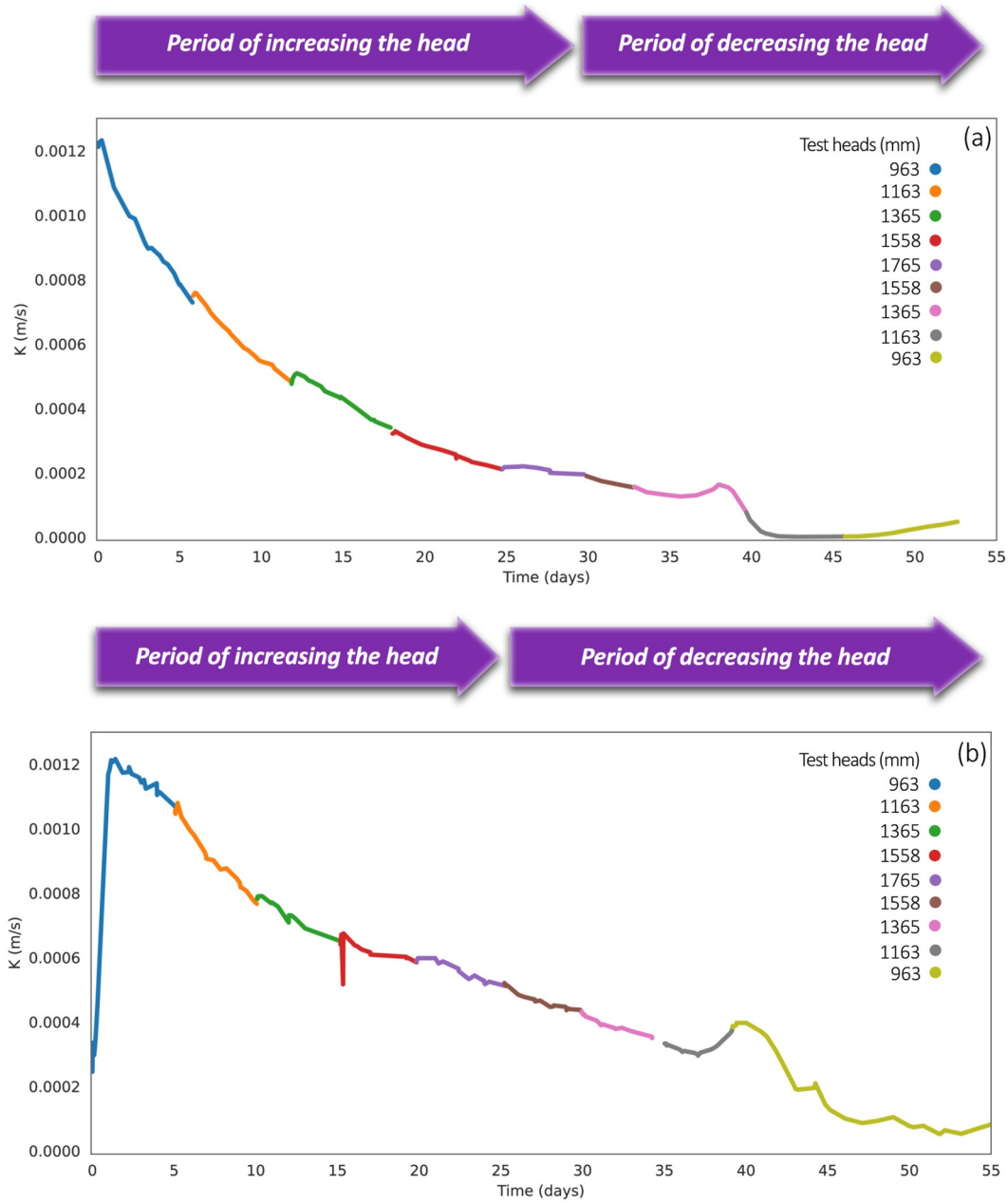

Figure 5. Changes of Ks over time for samples A (a) and B (b)- the generally reducing trend in Ks is noticeable in both samples.

4.2. Flow-Head Gradient Relationship

In the hypothetical scenario, where the samples remained unchanged throughout the tests, Darcy's law would anticipate the clustering of all data points at each hydraulic head increment around a single point, forming a unified line. Figure 6 illustrates the relationship between flow rate (Q) and hydraulic head gradient (i) within samples A and B across varying hydraulic head levels. The symbol "R" signifies the period characterized by a decreasing head. The scatterplots demonstrate the absence of a straightforward linear correlation between Q and i.

In the case of sample A, during test phases 1 to 4, wherein the head is incrementally raised every 5 or 6 days from 963 to 1,765 mm, a decrease in flow accompanied by an increase in head gradient becomes evident. Interestingly, even within each step, the scatterplot does not exhibit the expected convergence around a single point, as outlined

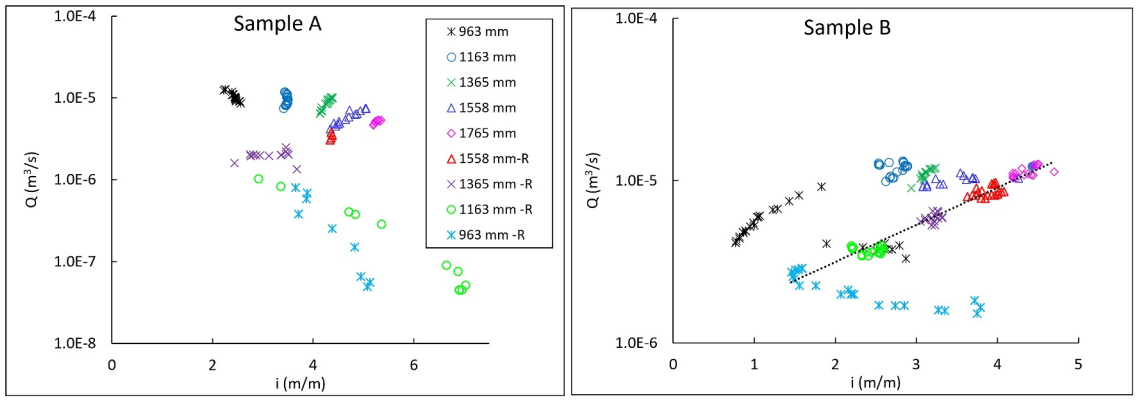

Figure 6. Scatterplots exploring the correlation between head gradient (i) and flow rate (Q) in samples A and B with different hydraulic head levels. The symbol "R" signifies the period characterized by a decreasing hydraulic head. Y axis is in logarithmic scale. A hypothetical line is added to the graph of sample B to show the linearity.

by Darcy's law. This suggests a dynamic nature of the sample during this period, with the saturated hydraulic conductivity undergoing continuous changes. However, Phase 5, characterized by the maximum head of 1,765 mm and a 5 day observation period, showcases a remarkable consistency in both head gradient and flow rate, implying a phase of stability.

Furthermore, as the head is reduced to 1,558 mm, this stability persists, with the scatterplot points clustering around a single location and both flow rate and head gradient diminishing. On the contrary, during phases 7 to 9, where the head drops from 1,365 to 963 mm, the scatterplot points display unpredictable distribution, deviating significantly from the expectations of Darcy's law. This observation indicates a departure from the anticipated behavior of the sample.

In sample B, the initial phase with a head of 963 mm shows an unexpected trend where both the head gradient and flow rate increase, deviating from the expected convergence around a single point. As we move through phases 2 to 4, involving a hydraulic head increase from 1,163 to 1,558 mm, a distinct behavior emerges: despite the elevated hydraulic head, the head gradient rises while the flow rate unexpectedly drops. This pattern suggests a shift in the hydraulic properties of the samples.

Nevertheless, when the hydraulic head is raised to 1,765 mm and subsequently reduced to 1,163 mm over four 5 day intervals, the sample aligns somewhat better with the predictions of Darcy's law. Data points cluster more closely around a central location, and the flow rate responds to changes in the hydraulic head. However, variations still exist at each step. In contrast, at the lowest head level of 963 mm, there's an increase in head gradient while the flow rate remains stable.

4.3. Sample a Behavior in a Relatively Short-Duration Test

Interestingly, this relatively quick test (Phase 10) demonstrated a strong linear correlation between the water flux and the gradient within the sample, as expected by the Darcy law. The saturated hydraulic conductivity was determined to be 1.53×10^{-4} m/s during the increasing stage of the test head and 1.75×10^{-4} m/s during the decreasing stage. The correlation between Q and i is illustrated in Figure 7. Contrary to Figure 6, a notably stronger correlation between Q and i can be observed.

4.4. Extending the Sample B in the Minimum Constant Head for 31 Days

Test B has been extended for an additional 31 day period under the minimum head condition (963 mm). This extension aims to investigate whether saturated hydraulic conductivity comes into stability without any disruptions.

Figure 8a depicts the correlation between flow rate and head gradient during extended Phase 9 period. The Q-i correlation exhibits unpredictable fluctuations in both hydraulic gradient and flow rate, mirroring the patterns observed in the preceding 45 days, as shown in Figure 6.

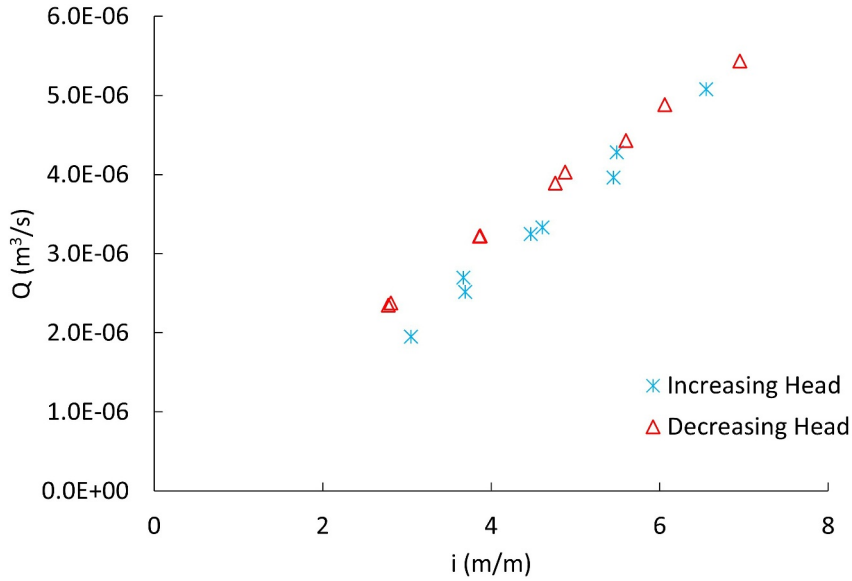

Figure 7. The relationship between Q and i in Phase 10 for sample A, where the gradients are varied. The blue and orange arrows represent the periods of increasing and decreasing test heads, respectively.

The temporal evolution of *Ks* is visually outlined in Figure 8b. The variability of *Ks* spans from 1.25×10^{-4} m/s to 0.5×10^{-4} m/s, centering around a median value of 1.0×10^{-4} m/s. In summary, the continuation of the testing procedure with a consistent hydraulic head maintained over the course of 31 days does not result in the stabilization of the saturated hydraulic conductivity of the sample. The *Ks* values persistently oscillate within a range of +33% and −46% around the median value, thereby underscoring the absence of stability in the system. However, a decreasing trend is absent in contrast to previous observation periods.

4.5. Comparison of Soil Properties Before and After the Tests

Figure 9 shows the *PSD* of the sample's top, middle, and bottom sections and the original sample prior to the test. Additionally, Table 3 compares the total particles below and above 75 μm for reference. The results in Table 3 indicate that the sample's total percentage of fine particles decreased after the tests. Approximately 2% of fine particles in sample *A* and 1% in sample *B* were washed away during the long-term tests which is negligible.

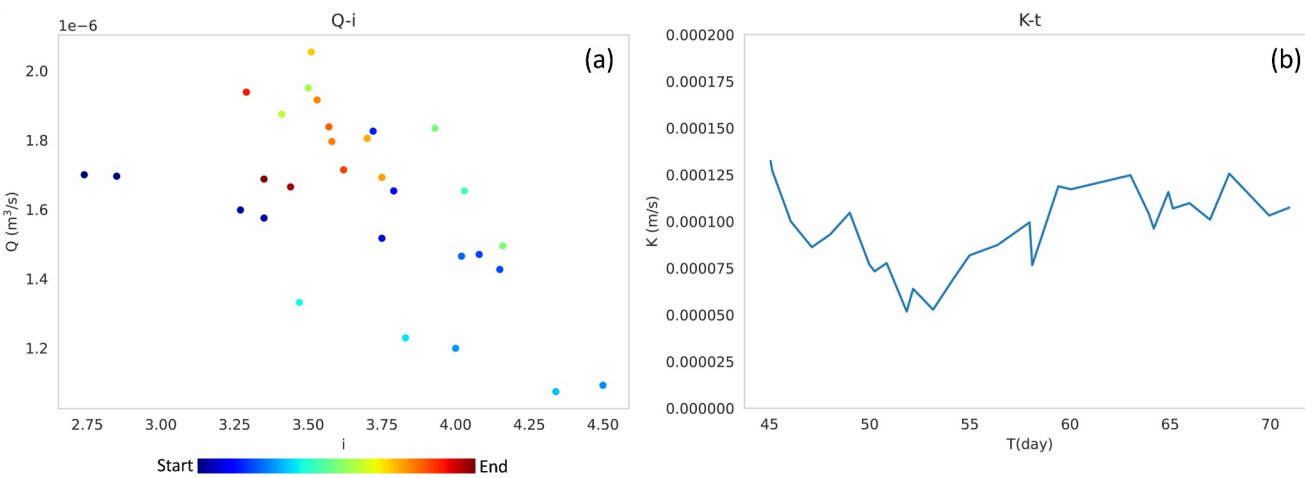

Figure 8. (a) The relationship between Q and i for sample B during an extended period (31 days) of running Phase 9 at the minimum hydraulic head. The color spectrum and arrows depict the temporal sequence of the measurements. (b) The changes in Ks over time for sample B during the same 31 day duration of Phase 9 at the minimum hydraulic head.

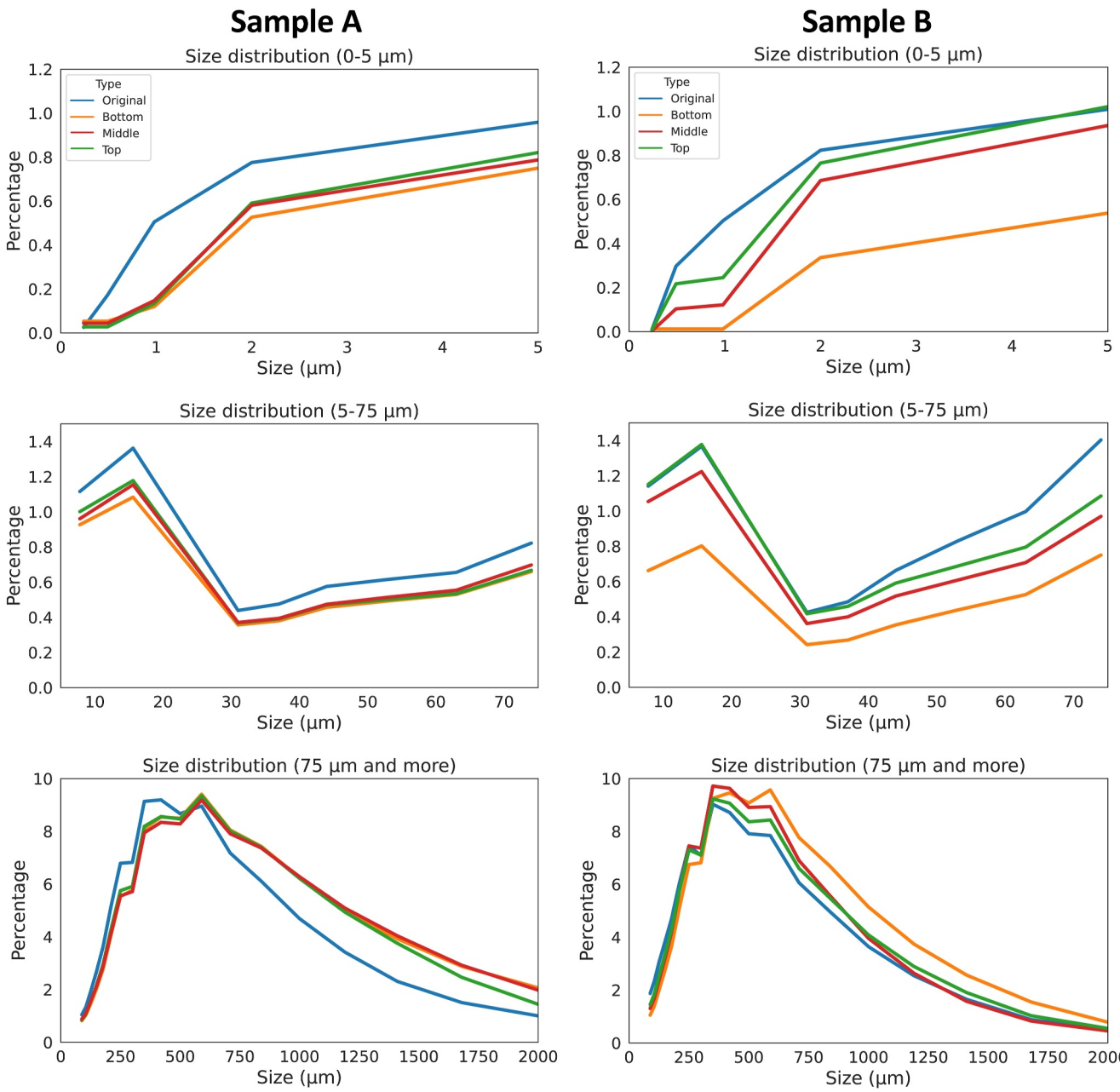

Figure 9. Particle size analysis of the samples (comparison of the samples before tests and after tests, divided by sub-samples of different sections).

Table 3
Comparison of Total Percentage of Particles Below and Above 75 μm Before and After Tests Divided by Different Sections in the Sample

	Sample A				Sample B			
Totals (%)	Original	Bottom	Middle	Top	Original	Bottom	Middle	Top
Below 75 μm	7.37	5.09	5.41	5.74	8.42	4.06	6.68	7.63
Above 75 μm	92.61	94.91	94.59	94.26	91.58	95.94	93.32	92.37

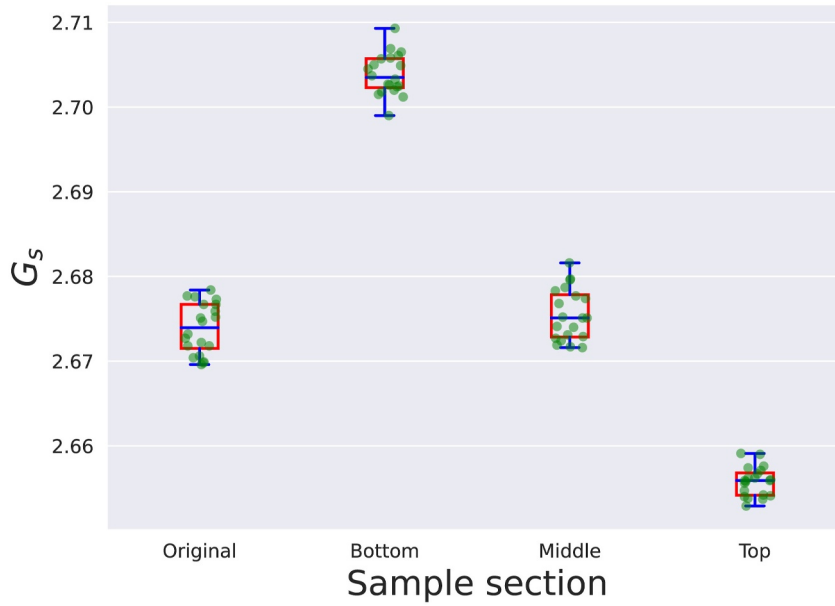

Figure 10. Gs (density of grains to the density of water) of sample A before and after test divided by sub-samples of different sections.

Measurements of saturated weight of the cells before and after the tests aligns with the particle size distribution data and confirms the latter. Because the rate of outflow was high during the tests, it was impossible to observe the fine particles leaving the sample or track the changes in the water color. It is noteworthy that samples *A* and *B* contained less than 9% of fine particles (below 75 μm).

Figure 9 and Table 3 show that the percentage of fine particles below 75 μm is highest at the top section of the samples, followed by the middle and bottom sections. The percentages of fine particles after finishing the tests for sample A is 5.09%, 5.41%, and 5.74% from bottom to top respectively. The percentages of fine particles for sample B are 4.06%, 6.68%, and 7.63% from bottom to top, respectively. While the difference in the percentage of fine particles among different sections is minor for sample A (less than 1%), it is higher for sample B (around 3%).

Gs measurements are presented as a box plot in Figure 10. The box plots illustrate notable changes in the specific gravity of the sample in comparison to the original sample. The lowest *Gs* is found at the top section of sample A with the mean value of 2.65, followed by 2.67 in the middle section, and 2.70 at the bottom. As can be seen from Figure 10, the *Gs* of middle section of the sample is close to the *Gs* before the tests being around 2.67. In conclusion, the highest *Gs* is observed at the bottom section, with a slight increase in the middle section, and the lowest at the top, compared to the *Gs* of the sample before the test.

5. Discussion

Examining soil properties in the original sample before and after the constant head test reveals notable alterations in the soil characteristics. These changes directly impact the saturated hydraulic conductivity, highlighting the direct influence of the test on soil properties and subsequent hydraulic behavior. For example, Figures 5a and 5b demonstrates a prevailing long-term decreasing trend in *Ks*. However, it is important to note that there are also intermittent shorter periods where *Ks* shows an increase. This observation highlights the dynamic nature of the system, wherein both long-term trends and shorter-term fluctuations in saturated hydraulic conductivity are evident.

There is a period of noticeable short increase in the *Ks* of both samples between days 35 and 40 (Figure 5). A similar temporary increase in the *Ks* was recorded by Vandevivere and Baveye (1992) and Du et al. (2018) during permeation of a sandy sample with an influent containing bacterial and chemical agents. However, they did not note the increase in their discussion. Subtle changes in the test set up can cause disturbance in the test and change *Ks*. In this research test set up was not changed during permeation. Additionally, the sudden increase of *Ks* occurs

in both samples. The movement and accumulation of fine particles can block the drainable pores, and consequently, the blockage increases the pressure in the blocked zone. Then the pressure builds up and it reaches to a critical point that unblocks the pore and the fine particles move to another zone in the sample, and hence, *Ks* increases. Then the particles rearrange, and *Ks* keeps reducing. This effect might repeat if the test keeps running for a longer period.

The *Ks* tests on the coarse particles (sandy samples with less than 10% fines) are generally short because the variation of *Ks* is very marginal during the first few hours of the tests. For example, in sample *A*, the change of *Ks* during the first 5 hr from starting the test was only 2%, which is negligible. However, after 5 days, the *Ks* dropped by 40%, and at the end of the test, the *Ks* dropped by around 96% from the beginning of the test.

The initial compaction moisture levels (8.1% for sample A and 11.8% for sample B) appear to have had limited influence on the extended-term variation of *Ks*. However, they might have played a role in the initial stages of permeation. As it can be seen from Figure 5, there is a relatively rapid period of spike in the *Ks* in sample B, which does not appear for sample A. There are marginal differences between sample A and B, including the PSD and dry bulk density. But the major difference is the initial compaction moisture, and the mentioned spike in sample B is related to the initial compaction moisture.

Also, throughout the head increase cycle, a notable pattern emerges: at the onset of each hydraulic head increment, there is a marginal uptick in *Ks*, which is subsequently followed by a sustained decrease. This minor elevation in *Ks* can be attributed to the abrupt rise in the hydraulic head.

Figure 6 clearly represents the dynamic nature of the samples' hydraulic gradient and pore pressure. These parameters undergo continuous fluctuations without exhibiting a consistent decreasing or increasing pattern. Even extending the test for a longer period (Figures 8(a) and 8(b)) does not create a stable gradient in the sample. Therefore, it can be inferred that the connectivity of the drainable pores is constantly changing. This observation underscores the complex behavior of the hydraulic system within the samples, emphasizing the need to consider the temporal variations in pore pressure when analyzing the overall hydraulic response. Nevertheless, in Figure 7 (Phase 10), representing a relatively quick test, the sample exhibits predominantly linear behavior. This underscores the limitations of quick tests in accurately assessing the *Ks*. It is essential to acknowledge, however, that Phase 10 commenced after Phase 9, during which all finer particles in preceding phases have undergone rearrangement.

The variations in the hydraulic gradient and discharge relation, and hence saturated hydraulic conductivity in the samples, can be attributed to several factors. According to the ASTM standard (ASTM D5856-15, 2015), air entrapment can potentially reduce saturated hydraulic conductivity. In this research, air entrapment in the sample was minimized during saturation. As a result, no visible evidence of air entrapment was observed during the test. The transparent acrylic test cell facilitated direct observation of the sample particles throughout the experiment. The absence of any noticeable formation of air bubbles among the particles from the sides of the samples suggests that air entrapment is unlikely to contribute to the observed reduction in *Ks* in our study.

Another factor that can affect the continuous reduction of *Ks* is the blockage of drainable pores with fine particles (Jeong et al., 2018), which restricts the flow of water and leads to a decrease in the *Ks*. Particle size distribution of the samples (Figure 9) and Table 3 show that the fine particles in all sections have decreased compared to the original sample prior to the test. This reduction is about 2% for sample A, and varies between 1% and 4.4% in sample B. Furthermore, there is a decrease in *Gs* in the top section and an increase in the bottom section (Figure 10). It can be concluded that mobile low-density fine particles (such as fine pumice) have displaced from the bottom of the sample to the top. Another reason for the reduction in the *Ks* can be related to the continuous blockage of the drainable pores with fine particles with rough surfaces (such as glass shards) or the simultaneous impact of blockage by glass shards and mobilization and blockage by low-density particles. The SEM image of the sample in Figure 11 shows a noticeable amount of glass shards and pumice in the small section of the sample. Continuous mobilization or re-deposition of these particles can change the connection of the drainable pores and reduce *Ks*.

The ASTM standard for granular soils (ASTM D2434-19, 2019) explains the procedure of estimating the *Ks* without mentioning the period of carrying out each test. Laboratory tests aimed at determining the *Ks* should account for the duration required for the specimen to attain a stable *Ks*. The standard cannot stipulate a fixed timeframe for achieving stable *Ks*, as each sample exhibits a distinct time requirement to reach this equilibrium.

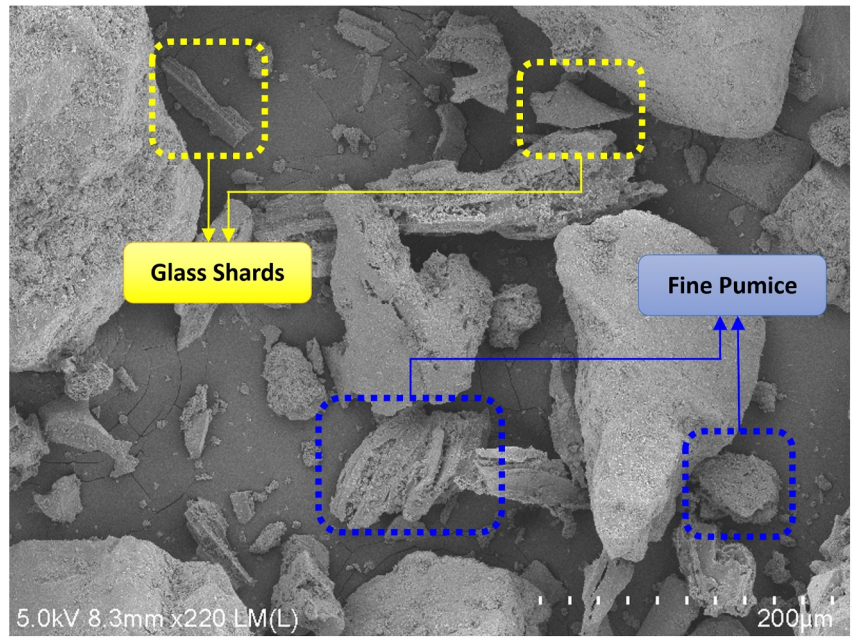

Figure 11. 220*x* magnification of the sample using SEM providing a closer view of the fine particles in the sample.

The mid to long-term *Ks* results in Figure 6 show a noticeable drop in the *Ks*, and if the test is terminated in a few hours, the resulting *Ks* will be 96% higher than the final one. Similar results were reported by Du et al. (2018) and Vanderzalm et al. (2020), when they permeated the sample with a solution containing *Fe (III)* or water with suspended solids. In our research, there was no *Fe (III)* contamination source, and the water used was drinking water from a tap. Figure 7 demonstrates a robust linear relationship between *Q* and *i* during the increasing and decreasing head phases during short-term testing. However, when comparing this figure to the long-term tests illustrated in Figure 6, it becomes evident that the *Q*-*i* relationship varies over time.

The long-term variability of saturated hydraulic conductivity holds significant importance for systems enduring extended saturation periods. The accurate estimation of *Ks* over the long-term plays a crucial role in modeling various hydrological processes, including infiltration, surface water runoff, soil erosion, and the design of drainage systems. Insight into *Ks* is essential for understanding and predicting the movement of water within soil systems, thereby informing effective management and engineering practices in these contexts. The findings of this investigation may serve as an initial reference for reevaluating the specification of saturated hydraulic conductivity in projects involving the backfilling of sandy materials subjected to prolonged saturation. Notably, this pertains to the substantial utilization of backfilled granular material in the construction of embankment dams (Tatone et al., 2009). These materials concurrently experience saturated conditions during reservoir water storage. Both the overestimation and underestimation of the saturated hydraulic conductivity of these materials can cause dam failure or incur additional expenses for backfilling and compaction. Additionally, sandy backfilled materials serve as filter components around subsurface drainage pipes and stormwater devices. Overestimating the saturated hydraulic conductivity of such filter materials may lead to reduced flow within the drainage system and increase surface ponding. Artificial soakage basins and soak pits are frequently recommended in the context of stormwater management in new urban developments (Shaver, 2020). These systems gather runoff from urban areas and gradually infiltrate the water into the ground. A crucial factor in designing these soakage systems is the saturated hydraulic conductivity. However, it's important to note that the testing duration commonly used to assess the *Ks* rate is often short and may not accurately represent the long-term behavior of saturated hydraulic conductivity. Consequently, it's wise to account for the long-term variation of Ks when reporting *Ks* values for applications involving soil saturation, such as soakage basins or drainage pipes. This precaution is essential as overestimation could lead to erroneous calculations.

Moreover, an array of studies has been conducted on pedotransfer functions, which establish relationships between soil properties, including void ratio, grain size, and pore size distribution, for the estimation of the *Ks*

(Boadu, 2000; Daneshian et al., 2021; Jabro, 1992; Tanaka et al., 2003; Wang et al., 2017). The pedotransfer functions were generally developed to estimate the *Ks* of non-plastic and sandy soils (Breyer, 1964; Hazen, 1892; Kenney et al., 1984; Kozeny, 1927), however there are few pedotransfer functions developed for plastic soil, as well (Mbonimpa et al., 2002). As these functions are usually developed based on *Ks* tests in the laboratory (Mbonimpa et al., 2002; Slichter, 1898; Terzaghi, 1925), comparing the variations of the Ks from this research with prediction of pedotransfer functions will reveal whether these functions are able to account for long-term changes of *Ks*.

6. Conclusion

This study provides valuable insights into the variation of saturated hydraulic conductivity in sandy samples through a long-term constant head experiment. To the knowledge of the authors, this is the first study that specifically focuses on the changes of the *Ks* over an extended period of time in the laboratory on sandy soils. The results demonstrate a significant reduction in *Ks*, primarily due to physical clogging caused by fines and pumice particles. The increased concentration of pumice particles in the top section indicates their mobility and potential blockage of drainable pore sections, affecting *Ks*. These changes were not observed in short-term tests, highlighting the importance of longer-term investigations. The findings stress the need for extended constant head tests to accurately assess and report *Ks* in sandy samples, enhancing our understanding of their hydraulic behavior.

Given that sand mixtures are employed for various construction purposes as backfill materials, which may remain saturated for extended periods, this study highlights the necessity of conducting extended constant head laboratory tests to accurately report the *Ks*. This research specifically investigates the variations in *Ks* for non-plastic sand containing less than 10% fine material, thereby limiting the generalizability of the findings to sandy soils of different origins. Consequently, it is recommended that extended constant head tests be performed on other soil types to explore the variations in *Ks*. Additionally, the pattern of changes in *Ks* can be further examined through the use of advanced technologies such as x-ray computed tomography (CT) during testing. CT scanning has the potential to elucidate particle movement within the sample, offering valuable insights into the migration of fine particles during testing, the changes in the connectivity of drainable pores within the specimen, and the subsequent impact of these changes on *Ks*.

Data Availability Statement

All data used and generated by this study, including hydraulic head and flow measurements, can be found in ZENODO repository (Ashouri, 2024).

Acknowledgments
This research was supported by the University of Waikato Doctoral Scholarship. Open access publishing facilitated by The University of Waikato, as part of the Wiley - The University of Waikato agreement via the Council of Australian University Librarians.

References

Ashouri, S. N. (2024). Supplementary Data for Manuscript "Examining the mid to long-term variability in saturated hydraulic conductivity of sandy soils and its influencing factors under constant head test in the laboratory.". https://doi.org/10.5281/zenodo.10538456

ASTM, W. C. P. (2012). *Standard test methods for laboratory compaction characteristics of soil using standard effort*. ASTM International. https://doi.org/10.1520/D0698-12E01

ASTM D2434-19. (2019). *Standard test method for permeability of granular soils (constant head)*. ASTM International. https://doi.org/10.1520/D2434-19

ASTM D2487. (2020). *Standard practice for classification of soils for engineering purposes (unified soil classification system)*. ASTM.

ASTM D5856-15. (2015). *Standard test method for measurement of hydraulic conductivity of porous material using a rigid-wall, compaction-mold permeameter*. ASTM International.

Ben-Hur, M., Yolcu, G., Uysal, H., Lado, M., & Paz, A. (2009). Soil structure changes: Aggregate size and soil texture effects on hydraulic conductivity under different saline and sodic conditions. *Australian Journal of Soil Research*, *47*(7), 688. https://doi.org/10.1071/SR09009

Boadu, F. K. (2000). Hydraulic conductivity of soils from grain-size distribution: New models. *Journal of Geotechnical and Geoenvironmental Engineering*, *126*(8), 739–746. https://doi.org/10.1061/(ASCE)1090-0241(2000)126:8(739)

Breyer, W. (1964). Zur Bestimmung der Wasserdurchlässigkeit von Kiesen und Sanden aus der Kornverteilung. *Wasserwirtschaft, Wassertechnik*, *14*, 165–169.

Cihan, A., Petrusak, R., Bhuvankar, P., Alumbaugh, D., Trautz, R., & Birkholzer, J. T. (2022). Permeability decline by clay fines migration around a low-salinity fluid injection well. *Ground Water*, *60*(1), 87–98. https://doi.org/10.1111/gwat.13127

Daneshian, B., Habibagahi, G., & Nikooee, E. (2021). Determination of unsaturated hydraulic conductivity of sandy soils: A new pore network approach. *Acta Geotechnica*, *16*(2), 449–466. https://doi.org/10.1007/s11440-020-01088-3

Dikinya, O., Hinz, C., & Aylmore, G. (2006). Dispersion and re-deposition of fine particles and their effects on saturated hydraulic conductivity. *Soil Research*, *44*(1), 47. https://doi.org/10.1071/SR05067

Du, X., Wang, Z., & Ye, X. (2013). Potential clogging and dissolution effects during artificial recharge of groundwater using potable water. *Water Resources Management*, *27*(10), 3573–3583. https://doi.org/10.1007/S11269-013-0365-5/FIGURES/13

Du, X., Zhang, H., Ye, X., & Lu, Y. (2018). Flow velocity effects on Fe(III) clogging during managed aquifer recharge using urban storm water. *Water*, *10*(4), 358. https://doi.org/10.3390/W10040358

Fang, Y., Kong, L., Zhang, P., Zhang, L., Zhao, H., Xiang, X., et al. (2022). Fifteen-year analysis of constructed wetland clogging: A critical review. *Journal of Cleaner Production*, *365*, 132755. https://doi.org/10.1016/j.jclepro.2022.132755

Francisca, F. M., & Glatstein, D. A. (2010). Long term hydraulic conductivity of compacted soils permeated with landfill leachate. *Applied Clay Science*, *49*(3), 187–193. https://doi.org/10.1016/j.clay.2010.05.003

Hazen, A. (1892). Some physical properties of sands and gravels, with special reference to their use in filtration. *24th Annual Report, Massachusetts State Board of Health*, 539–556.

Hwang, H. T., Jeen, S. W., Suleiman, A. A., & Lee, K. K. (2017). Comparison of saturated hydraulic conductivity estimated by three different methods. https://doi.org/10.3390/w9120942

Jabro, J. D. (1992). Estimation of saturated hydraulic conductivity of soils from particle size distribution and bulk density data. *Transactions of the ASAE*, *35*(2), 557–560. https://doi.org/10.13031/2013.28633

Jeong, H. Y., Jun, S.-C., Cheon, J.-Y., & Park, M. (2018). A review on clogging mechanisms and managements in aquifer storage and recovery (ASR) applications. *Geosciences Journal*, *22*(4), 667–679. https://doi.org/10.1007/s12303-017-0073-x

Jo, H. Y., Benson, C. H., Shackelford, C. D., Lee, J.-M., & Edil, T. B. (2005). Long-term hydraulic conductivity of a geosynthetic clay liner permeated with inorganic salt solutions. *Journal of Geotechnical and Geoenvironmental Engineering*, *131*(4), 405–417. https://doi.org/10.1061/(asce)1090-0241(2005)131:4(405)

Kenney, T. C., Lau, D., & Ofoegbu, G. I. (1984). Permeability of compacted granular materials. *Canadian Geotechnical Journal*, *21*(4), 726–729. https://doi.org/10.1139/t84-080

Konikow, L. F., August, L. L., & Voss, C. I. (2001). Effects of clay dispersion on aquifer storage and recovery in coastal aquifers. *Transport in Porous Media*, *43*(1), 45–64. https://doi.org/10.1023/A:1010613525547

Kozeny, J. (1927). Ueber kapillare Leitung des Wassers im Boden. *Sitzungsber Akad*, 271–306.

Kretzschmar, R., Borkovec, M., Grolimund, D., & Elimelech, M. (1999). Mobile subsurface colloids and their role in contaminant transport. *Advances in Agronomy*, 121–193. https://doi.org/10.1016/S0065-2113(08)60427-7

Ladd, R. (1978). Preparing test specimens using undercompaction. *Geotechnical Testing Journal*, *1*(1), 16–23. https://doi.org/10.1520/GTJ10364J

Landcare Research. (2023). *SMAP (digital soil Map of New Zealand)*. Landcare Research. (Manaaki Whenua).

Li, K., Chen, Y., Ye, W., & Wang, Q. (2023). Modelling the evolution of dual-pore structure for compacted clays along hydro-mechanical paths. *Computers and Geotechnics*, *157*, 105308. https://doi.org/10.1016/j.compgeo.2023.105308

Liu, Y., & Liu, J. (2020). The BioChemical clogging of landfill leachate collection system: Based on laboratory studies. *International Journal of Environmental Research and Public Health*, *17*(7), 2299. https://doi.org/10.3390/ijerph17072299

Lu, H., Wang, C., Li, D., Li, J., & Wan, Y. (2020). Permeability, pore, and structural parameters of undisturbed silty clay presented in landfill leachate. *Water, Air, and Soil Pollution*, *231*(5), 190. https://doi.org/10.1007/s11270-020-04568-0

Mays, D. C., & Hunt, J. R. (2005). Hydrodynamic aspects of particle clogging in porous media. *Environmental Science and Technology*, *39*(2), 577–584. https://doi.org/10.1021/es049367k

Mbonimpa, M., Aubertin, M., Chapuis, R. P., & Bussière, B. (2002). Practical pedotransfer functions for estimating the saturated hydraulic conductivity. *Geotechnical & Geological Engineering*, *20*(3), 235–259. https://doi.org/10.1023/A:1016046214724

Mohan, K. K., Vaidya, R. N., Reed, M. G., & Fogler, H. S. (1993). Water sensitivity of sandstones containing swelling and non-swelling clays. *Colloids and Surfaces A: Physicochemical and Engineering Aspects*, *73*, 237–254. https://doi.org/10.1016/0927-7757(93)80019-B

Montoro, M. A., & Francisca, F. M. (2010). Soil permeability controlled by particle-fluid interaction. *Geotechnical & Geological Engineering*, *28*(6), 851–864. https://doi.org/10.1007/s10706-010-9348-y

Shaver, E. (2020). Waikato stormwater management guideline.

Siriwardene, N., Deletic, A., & Fletcher, T. (2007). Clogging of stormwater gravel infiltration systems and filters: Insights from a laboratory study. *Water Research*, *41*(7), 1433–1440. https://doi.org/10.1016/j.watres.2006.12.040

Slichter, C. (1898). Theoretical investigation of the motion of ground waters. *U.S. Geological Survey, 19th Annual Report*.

Song, W., Liu, X., Zheng, T., & Yang, J. (2020). A review of recharge and clogging in sandstone aquifer. *Geothermics*, *87*, 101857. https://doi.org/10.1016/j.geothermics.2020.101857

Suleiman, A. A., & Ritchie, J. T. (2001). *Estimating saturated hydraulic conductivity from soil porosity*. Transactions of the American Society of Agricultural Engineers. https://doi.org/10.13031/2013.4683

Tanaka, H., Shiwakoti, D. R., Omukai, N., Rito, F., Locat, J., & Tanaka, M. (2003). Pore size distribution of clayey soils measured by mercury intrusion porosimetry and its relation to hydraulic conductivity. *Soils and Foundations*, *43*(6), 63–73. https://doi.org/10.3208/sandf.43.6_63

Tangparitkul, S., Saul, A., Leelasukseree, C., Yusuf, M., & Kalantariasl, A. (2020). Fines migration and permeability decline during reservoir depletion coupled with clay swelling due to low-salinity water injection: An analytical study. *Journal of Petroleum Science and Engineering*, *194*, 107448. https://doi.org/10.1016/j.petrol.2020.107448

Tatone, B., Donnelly, C. R., Protulipac, D., & Clarke, C. (2009). Evaluation of the hydraulic efficiency of a newly constructed plastic concrete cut-off wall. *Proceedings of the 2009 Canadian Dam Association Conference*. https://doi.org/10.13140/2.1.3540.1284

Terzaghi, C. (1925). *Principles of soil mechanics* (pp. 95–832). Engineering News Record.

Torkzaban, S., Bradford, S. A., Vanderzalm, J. L., Patterson, B. M., Harris, B., & Prommer, H. (2015). Colloid release and clogging in porous media: Effects of solution ionic strength and flow velocity. *Journal of Contaminant Hydrology*, *181*, 161–171. https://doi.org/10.1016/j.jconhyd.2015.06.005

Touze-Foltz, N., Duquennoi, C., & Gaget, E. (2006). Hydraulic and mechanical behavior of GCLs in contact with leachate as part of a composite liner. *Geotextiles and Geomembranes*, *24*(3), 188–197. https://doi.org/10.1016/j.geotexmem.2006.01.004

Valencia-González, Y., Quintero-Ramírez, A., & Lara-Valencia, L. A. (2022). A laboratory methodology for predicting variations in the geotechnical parameters of soil exposed to solid waste leachates in the field. *Results in Engineering*, *14*, 100398. https://doi.org/10.1016/j.rineng.2022.100398

Vanderzalm, J. L., Page, D. W., Barry, K. E., & Gonzalez, D. (2020). Evaluating treatment requirements for recycled water to manage well clogging during aquifer storage and recovery: A case study in the werribee formation, Australia. *Water*, *12*(9), 2575. https://doi.org/10.3390/W12092575

Vandevivere, P., & Baveye, P. (1992). Effect of bacterial extracellular polymers on the saturated hydraulic conductivity of sand columns. *Applied and Environmental Microbiology*, *58*(5), 1690–1698. https://doi.org/10.1128/aem.58.5.1690-1698.1992

VanGulck, J. F., & Rowe, R. K. (2004). Evolution of clog formation with time in columns permeated with synthetic landfill leachate. *Journal of Contaminant Hydrology*, *75*(1–2), 115–139. https://doi.org/10.1016/j.jconhyd.2004.06.001

Wang, B., Chen, L., & Niu, Z. (2022). Critical hydraulic gradient and fine particle migration of sand under upward seepage flow. *Scientific Reports*, *12*(1), 14440. https://doi.org/10.1038/s41598-022-18720-9

Wang, H., Qian, H., & Gao, Y. (2020). Non-darcian flow in loess at low hydraulic gradient. *Engineering Geology*, *267*, 105483. https://doi.org/10.1016/j.enggeo.2020.105483

Wang, J., François, B., & Lambert, P. (2017). Equations for hydraulic conductivity estimation from particle size distribution: A dimensional analysis. *Water Resources Research*, *53*(9), 8127–8134. https://doi.org/10.1002/2017WR020888

Wang, W., Dong, L., Zhai, T., Wang, W., Wu, H., Kong, F., et al. (2023). Bio-clogging mitigation in constructed wetland using microbial fuel cells with novel hybrid air-photocathode. *Science of the Total Environment*, *881*, 163423. https://doi.org/10.1016/j.scitotenv.2023.163423

Wang, Y., Yu, M., Bo, Z., Bedrikovetsky, P., & Le-Hussain, F. (2021). Effect of temperature on mineral reactions and fines migration during low-salinity water injection into Berea sandstone. *Journal of Petroleum Science and Engineering*, *202*, 108482. https://doi.org/10.1016/j.petrol.2021.108482

Wang, Z., Du, X., Yang, Y., & Ye, X. (2012). Surface clogging process modeling of suspended solids during urban stormwater aquifer recharge. *Journal of Environmental Sciences*, *24*(8), 1418–1424. https://doi.org/10.1016/S1001-0742(11)60961-3

Ye, X., Cui, R., Du, X., Ma, S., Zhao, J., Lu, Y., & Wan, Y. (2019). Mechanism of suspended kaolinite particle clogging in porous media during managed aquifer recharge. *Ground Water*, *57*(5), 764–771. https://doi.org/10.1111/gwat.12872